

Spin-density functional theories and their $+U$ and $+J$ extensions: a comparative study of transition metals and transition metal oxides

Hanghui Chen^{1,2} and Andrew J. Millis¹

¹*Department of Physics,*

Columbia University,

New York, NY, 10027, USA

²*Department of Applied Physics and Applied Mathematics,*

Columbia University,

New York, NY, 10027, USA

(Dated: November 20, 2015)

Abstract

Previous work on the physical content of exchange correlation functionals that depend on both charge and spin densities is extended to elemental transition metals and a wider range of perovskite transition metal oxides. A comparison of spectra and magnetic moments calculated using exchange correlation functionals depending on charge density only or on both charge and spin densities, as well as the $+U$ and $+J$ extensions of these methods confirms previous conclusions that the spin-dependent part of the exchange correlation functional provides an effective Hund's interaction acting on the transition metal d orbitals. For the local spin density approximation and spin-dependent Perdew-Burke-Ernzerhof generalized gradient approximation, the effective Hund's exchange is found to be larger than 1 eV. The results indicate that at least as far as applications to transition metals and their oxides are concerned, $+U$, $+J$ and +dynamical mean field theory extensions of density functional theory should be based on exchange-correlation functionals of charge density only.

I. INTRODUCTION

Density functional theory (DFT) is an enormously successful and powerful method for treating the properties of interacting electrons in atoms, molecules and solids [1]. In its original form, DFT was based on the minimization of a functional of the space-dependent electronic charge density [2], but soon after, extensions to functionals depending on the spin density as well as the charge density were introduced [3, 4]. These functionals are not exactly known, but current approximations to the charge-density-only functional such as the local density approximation (LDA) [3] and the generalized gradient approximation (GGA) [5] provide a very good representation of the electronic properties of many materials. Spin dependent extensions of the local density approximation (LSDA) [4, 6, 7] and of the generalized gradient approximation (sGGA) [8, 9] provide important insights into magnetic properties of many materials. However, the currently available implementations of DFT have difficulty dealing with phenomena associated with strong electronic correlations, including magnetism and metal-insulator transitions [10], associated with partly filled transition metal *d*-shells or partly filled lanthanides *f*-shells. These difficulties have motivated extensions of the original density functional idea to explicitly include additional interaction terms amongst physically relevant orbitals such as transition metal *d*-orbitals [11, 12]. Loosely speaking, the extra interactions consist of a term, typically referred to as “*U*”, that couples to the square of the total occupancy of the selected orbitals and a set of terms, typically referred to as “*J*”, that distinguish different multiplets at fixed total occupancy of the *d*-shells. When the interaction effects are treated within a Hartree-Fock approximation, the extensions are typically referred to as “+*U*” and “+*J*” methods. When the interaction physics is solved via the dynamical mean field method, the extension [13–15] is referred to as “+DMFT”.

A key aspect of correlation physics in transition metals and their oxides is the formation and dynamics of local moments arising from electrons in partially filled transition metal *d*-shells. Both the spin-dependent DFT (sDFT) methods and the +*U*/+*J* extensions of DFT express important aspects of this physics, and a combined sDFT+*U*+*J* methodology seems an attractive approach to strong correlation physics. However, recent studies indicate that this combination produces seemingly unphysical behavior, including an unreasonable *J*-dependence of structural parameters in nickelates [16, 17] and of the high-spin/low-spin energy difference in a spin crossover molecule [18]. A study by Park, Marianetti and one

of us [17] on beyond-DFT theories for the rare earth nickelates led to the conclusion that a source of the difficulty was that the sDFT theories contain an effective J acting on the Ni d -states that is already larger than the value considered to be reasonable for transition metals.

In this paper we extend the analysis of Ref. [17] to wider classes of materials and additional observables. We study SrMnO_3 (an antiferromagnetic insulator with a d^3 formal valence, of current interest for potential multiferroic behavior [19, 20]), SrVO_3 (a moderately correlated metal with formal transition metal valence d^1), and elemental Fe. For completeness we also present results for the previously studied LaNiO_3 . We restrict attention to a Hartree-Fock treatment of the additional correlations (i.e. consider only $+U/+J$ extensions but not +DMFT, although we expect our conclusions will apply to that case also). We compute energy differences between ferromagnetic and antiferromagnetic states as well as magnetic moments. Further, we display the spin-dependent density of states, which provides insight into the issues. Following Ref. [17], we compare results obtained from sDFT theories to results of sDFT+ $U+J$ and DFT+ $U+J$ theories. We find that DFT+ $U+J$ with $J \sim 1$ -1.5 eV reproduces most aspects of sDFT+ U ($J = 0$) calculations, confirming that the conclusions of Ref. [17] apply to a wide range of transition metal-based materials. We show explicitly that in these systems, the $+U/+J$ extensions of charge-density-only DFT provide a better description of the physical properties than $+U/+J$ extensions of sDFT.

The rest of this paper is organized as follows. Sec. II presents the formalism we use. Sec. III presents energy differences between different magnetic states and magnetic moments for ferromagnetic and antiferromagnetic states. Sec. IV presents an analysis of calculated densities of states. Sec. V is a summary and conclusion.

II. FORMALISM

A. Theoretical Approach

Density functional theory (DFT) and spin-dependent density functional theory (sDFT) and their $+U$ and $+J$ extensions are based on extremization of functionals of charge density $n(\mathbf{r})$, spin density $m(\mathbf{r})$ and the reduced density matrix describing the charge n_a and spin m_a state of designated correlated orbitals labelled by a . The extremization is actually

accomplished by solving a Schrödinger equation involving an exchange-correlation potential V_{XC} which depends on $n(\mathbf{r})$ (in the case of DFT) or on $n(\mathbf{r})$ and $m(\mathbf{r})$ (in the case of sDFT) and an additional functional that depends on the orbital occupancies and on the interaction parameters (local- d and intra- d orbitals in the usual applications to transition metals and their oxides): schematically $V_U(n_a, m_a; U, J)$. An important part of the additional functional is a double counting correction V_{DC} that removes from V_{XC} the terms that are present in V_U . Thus in the “DFT+” methodologies V_{DC} does not have spin dependence, whereas in the “sDFT+” methodologies it does.

The known exchange-correlation functionals depend on the full charge (spin) density, the portion pertaining to the designated correlated orbitals cannot be extracted and the double counting correction thus cannot be rigorously derived [21]. The double counting term must be specified by approximate, phenomenologically based arguments. Different forms have been introduced [22, 23]. In this study, we use the widely-adopted fully localized limit (FLL) form. However, our basic conclusions are independent of the precise form chosen.

For the case of DFT+ $U+J$, the FLL double counting correction reads:

$$V_{DC} = U \left(N_d - \frac{1}{2} \right) - J \left(\frac{1}{2} N_d - \frac{1}{2} \right) \quad (1)$$

where N_d is the total occupancy of designated correlated orbitals (here transition metal d orbitals). U is the Hubbard U and J is the Hund’s coupling, which are the standard inputs of DFT+ $U+J$ calculations.

For the case of sDFT+ $U+J$, V_{DC} is spin dependent and the explicit FLL double counting form reads:

$$V_{DC}^\sigma = U \left(N_d^\sigma - \frac{1}{2} \right) - J \left(N_d^\sigma - \frac{1}{2} \right) \quad (2)$$

where N_d^σ is the total occupancy of designated orbitals with spin σ . $N_d = \sum_\sigma N_d^\sigma$. U and J have the same meaning as in Eq. (1). For non-magnetic cases, $N_d^\sigma = \frac{1}{2} N_d$ and Eq. (2) reduces to Eq. (1).

In our studies we compare two forms of $V_{XC}(n(\mathbf{r}))$: the local density approximation (LDA) [3] and the generalized gradient approximation (GGA) with the Perdew-Burke-Ernzerhof (PBE) parametrization [24]. Correspondingly for the spin-dependent density functionals, we use the local spin density approximation (LSDA) [3] and the spin-dependent

GGA with the PBE parametrization (sPBE) [24]. For the $+U$ and $+J$ extensions, we use the rotationally invariant Hubbard/Hund’s corrections introduced by Liechtenstein *et. al.* [12].

We note that DFT+ $U+J$ and sDFT+ $U+J$ methods become equivalent if applied to non-magnetic states ($m(\mathbf{r}) = m_a = 0$). For magnetic materials, the two methods differ in principle because in the DFT+ $U+J$ case only the spin-dependence of the correlated orbitals (here transition metal d orbitals) contributes to the spin dependence of the self-consistent potential felt by electrons. This is because the exchange-correlation potential depends only on the total charge density, so it yields a spin-independent contribution to the potential. In contrast, in the sDFT+ $U+J$ case the spin-dependence of the exchange-correlation potential means that the spin polarization of the non- d orbitals also contributes to the spin-dependence of the self-consistent potential. However we shall see that for the situations we consider, this difference is unimportant in practice, probably because the polarization of the non-correlated orbitals is small. The key difference between different choices of exchange-correlation functionals will be seen to be the magnitude of the spin-dependent term acting on the correlated orbitals.

B. Computational Details

We present results for representative transition metal oxides: cubic SrMnO₃, cubic SrVO₃ and pseudo-cubic LaNiO₃ (the last compound was previously studied in Ref. [17] and we reproduce the results for comparison) and one representative transition metal: iron. The simulation cell is illustrated in Fig. 1. For transition metal oxides, it consists of two perovskite primitive cells (10 atoms in total) stacked along the [111] direction (panels **A** of Fig. 1). For transition metal, we study body-centered iron (panels **B** of Fig. 1). For both transition metal oxides and transition metals, the computational cell can accommodate both ferromagnetic ordering and G -type (two-sublattice Néel) antiferromagnetic ordering. We use experimental lattice constants, respectively 3.80 Å (SrMnO₃ [25]), 3.84 Å (SrVO₃ [26]) and 3.86 Å (LaNiO₃ [27]) and 2.86 Å (Fe [28]).

The density functional theory calculations [2, 3] are performed within the *ab initio* plane-wave approach [29], as implemented in the Vienna Ab-initio Simulation Package (VASP) [30]. We employ projector augmented wave (PAW) pseudopotentials [31, 32]. We use an energy cutoff 600 eV and a $10 \times 10 \times 10$ Monkhorst-Pack grid. A higher energy

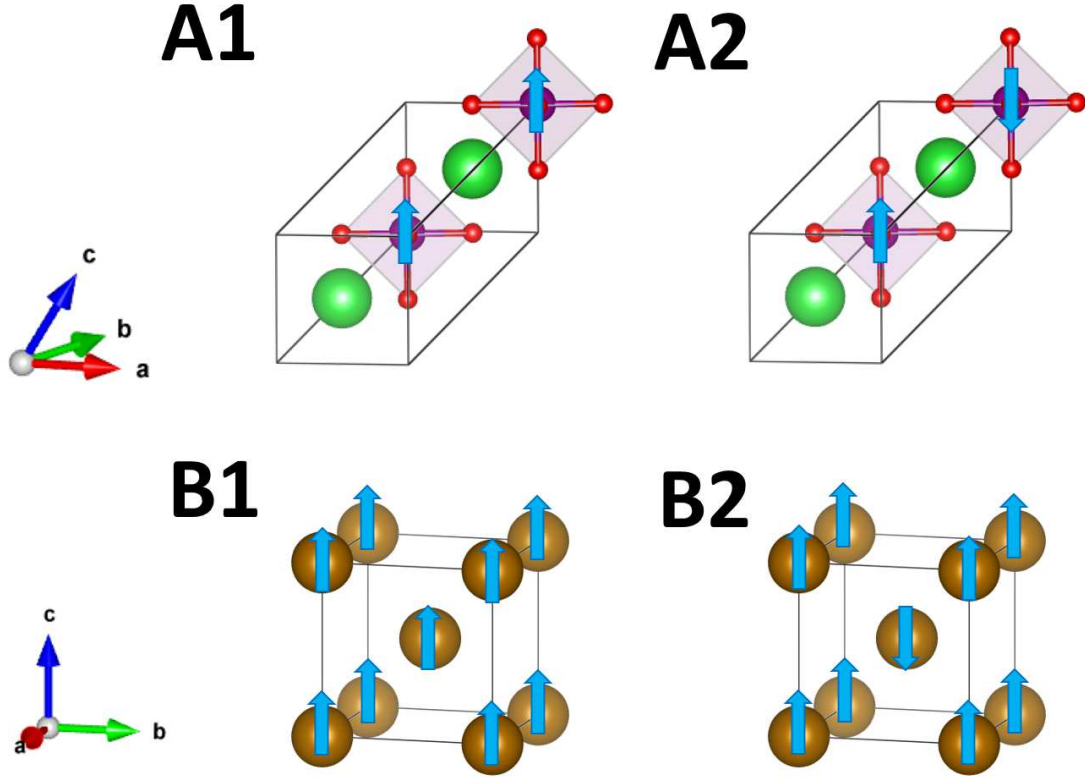


FIG. 1: Computational unit cells showing atoms (balls) and spin alignments (arrows). Panel **A**: simulation cell for transition metal oxides AMO_3 . The two perovskite unit cells are stacked along the $[111]$ direction. The A -site ion ($A = \text{La}$ or Sr in the current study) is the large ball (green on-line) and the intermediate-sized ball (purple on-line) represents the transition metal (M) ion ($M = \text{Mn}$, V or Ni in the current study). The small balls (red on-line) represent oxygen atoms. Panel **B**: simulation cell for body-centered iron. Column **1**: ferromagnetic ordering and column **2**: G -type antiferromagnetic ordering.

cutoff (800 eV) and a denser k -point sampling ($12 \times 12 \times 12$) are used to test the convergence and no significant difference is found. All the calculations allow for the possibility of spin-polarization to study different types of long-range magnetic orderings (if they can be stabilized). $\text{LDA}+U+J$ and $\text{PBE}+U+J$ are implemented in VASP as $\text{LDAUTYPE}=4$ and $\text{LSDA}+U+J$ and $\text{sPBE}+U+J$ are implemented in VASP as $\text{LDAUTYPE}=1$.

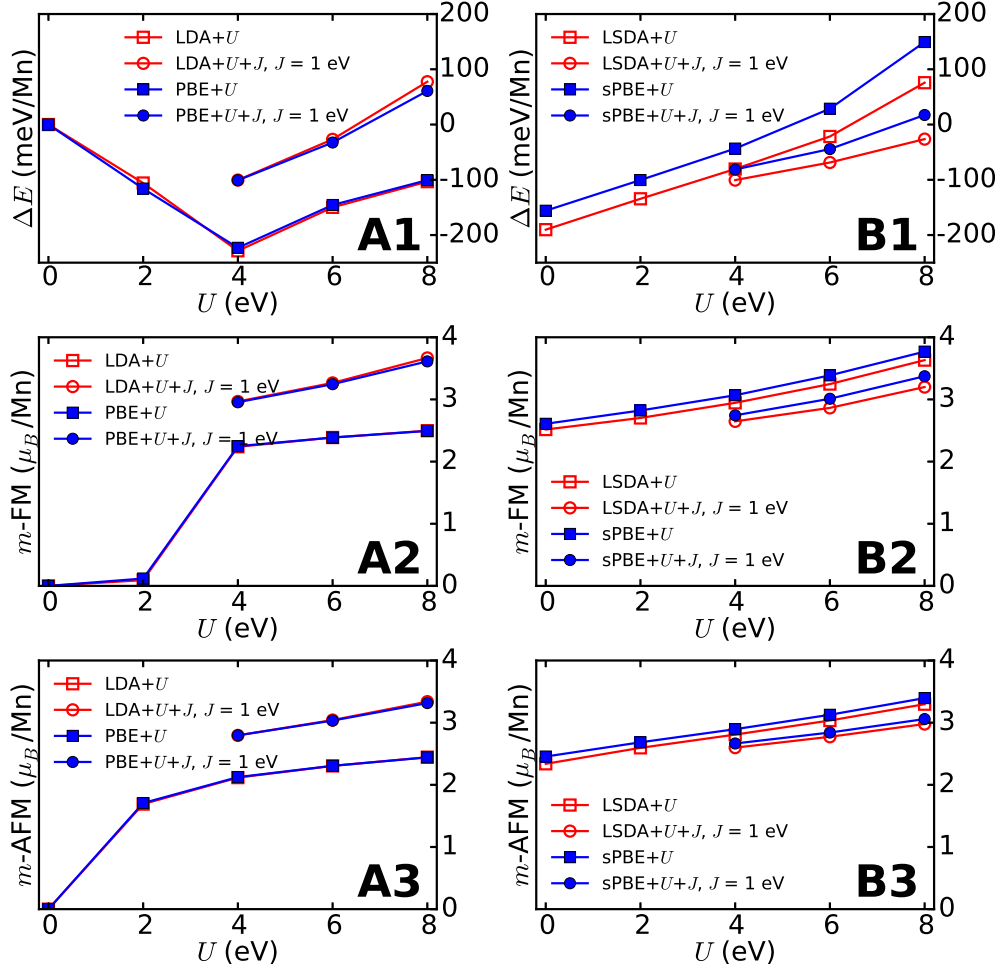


FIG. 2: Comparison of predictions from LDA+ U + J /PBE+ U + J (panels **A**) and LSDA+ U + J /sPBE+ U + J (panels **B**) methods for ground state properties of cubic SrMnO₃. Row **1**: energy difference $\Delta E = E(G) - E(F)$ between ferromagnetic (F) and G -type antiferromagnetic (G) ordering. Row **2**: magnetic moment per Mn of ferromagnetic state. Row **3**: magnetic moment per Mn of G -type antiferromagnetic state.

III. MAGNETIZATION AND ENERGY DIFFERENCES

In this section, we consider the ferromagnetic-antiferromagnetic energy differences and local magnetic moments in the ferromagnetic and antiferromagnetic states obtained using different methods. We begin with SrMnO₃, a cubic perovskite antiferromagnetic insulator

known experimentally [25] to exhibit an approximately a high-spin d^3 configuration with a fully spin-polarized t_{2g} shell and a nearly empty e_g shell.

Panel **A1** of Fig. 2 presents the energy difference between G -type (two sublattice Néel) antiferromagnetic and ferromagnetic states calculated using the DFT+ U + J method with two choices of exchange-correlation potential: the local density approximation (LDA) and the generalized gradient approximation in the Perdew-Burke-Ernzerhof parameterization (PBE). Panels **A2**, **A3** present the local magnetic moments of the ferromagnetic and antiferromagnetic states, respectively. We require that the net on-site interaction is repulsive: this imposes the constraint that $U > 3J$. Therefore, for $J = 1$ eV, we only consider $U > 3$ eV. In the DFT+ U + J method, there is no intrinsic exchange splitting in the exchange correlation functionals.

We see immediately that the two density functionals, LDA and PBE, give essentially identical results. For pure LDA and PBE ($U = J = 0$), SrMnO₃ is predicted to be non-magnetic. For moderate $U = 2$ eV, the ground state is antiferromagnetic and a ferromagnetic state could not be stabilized. For larger $U \gtrsim 4$ eV, the ferromagnetic state is locally stable. For sufficiently large U , the ground state is ferromagnetic. Increasing J favors ferromagnetism. For $U < 4$ eV, the calculated moments are substantially below the experimental value of $2.6 \mu_B/\text{Mn}$ [33]. We therefore believe that to adequately represent the physics of SrMnO₃ within the DFT+ U + J method a $U \gtrsim 4$ eV is required. For sufficiently large U and J ($J \gtrsim 1$ eV for $U = 6$ eV or $J \gtrsim 0.8$ eV for $U = 8$ eV), the calculated ground state of SrMnO₃ is ferromagnetic instead of experimentally observed G -type antiferromagnetic. We therefore believe that $U \lesssim 8$ eV is required within this method.

Magnetism arises from a Hartree treatment of the U interaction, supplemented by the tendency of the J term to favor high-spin states. As U is increased above $U = 4$ eV or J is increased from $J = 0$, the energy of the ferromagnetic state decreases relative to that of the antiferromagnetic state. The change in energy of the two states can be explained in terms of the energy dependence of the relevant exchange processes. Antiferromagnetism results from an inter- t_{2g} superexchange $\sim t^2/(U + 3J)$ where t is the hopping, while ferromagnetism comes from double exchange mediated by virtual occupancy of the e_g and proportional to t . As U and J are increased, the antiferromagnetic interaction thus weakens and above some critical U_c and J_c , the ferromagnetic interaction dominates.

We next consider the predictions of the spin dependent density functionals, shown in the

panels **B** of Fig. 2. We first observe that LSDA+ $U+J$ and sPBE+ $U+J$ produce different results, with sPBE+ $U+J$ favoring ferromagnetism more than LSDA+ $U+J$ and predicting slightly larger moments. Even without the + $U/+J$ corrections, pure LSDA and sPBE stabilize both ferromagnetic and antiferromagnetic states with local magnetic moments close to the experimental values. We interpret this result as indicating that the spin-dependent functionals possess an intrinsic exchange splitting that is large enough to separate the lower and upper Hubbard bands of Mn- d states, consistent with previous findings of Ref. [17] in the context of rare earth nickelates. We also comment that it is widely known [34–37] that sPBE gives a reasonable description of magnetic properties of $\text{La}_{1-x}\text{Sr}_x\text{MnO}_3$ (in particular, the magnetic transition point around $x = 0.5$), while adding U to sPBE impairs the agreement between theory and experiment. However, on the other hand, the physical U on Mn d -orbitals is definitely nonzero (around 4 eV from constrained random phase approximation calculations, cRPA [38]). Our results provide a natural explanation that the intrinsic “ J ” in the sPBE already produces a large enough spin-splitting and adding U further splits spin channels, which thus leads to some unphysical results. Using LDA+ $U+J$ /PBE+ $U+J$, we find that a physical range of U is between 4 and 8 eV, which is more consistent with previous cRPA calculations.

As was found in DFT+ $U+J$ calculations, increasing U in sDFT+ $U+J$ decreases the energy difference between the antiferromagnetic and ferromagnetic states, so that for large enough U the ferromagnetic state becomes favored. However, in contrast to DFT+ $U+J$, increasing J in sDFT+ $U+J$ *destabilizes* the ferromagnetic state. This counterintuitive result is similar to the previous finding of J -dependence of the high-spin/low-spin transition point in a spin crossover molecule [18] and is discussed in more detail in the next section.

To further investigate the differences between DFT+ $U+J$ and sDFT+ $U+J$ methods and to understand the robustness of our results across the perovskite family of materials, we present in Fig. 3 the ferromagnetic-antiferromagnetic energy difference $E(G) - E(F)$ of different transition metal oxides, calculated using sDFT+ U (with $J = 0$) and DFT+ $U+J$ (with $J = 1$ eV). We compare SrMnO_3 (antiferromagnetic insulator with half-filled t_{2g} -shell), SrVO_3 (moderately correlated metal) and LaNiO_3 (negative charge-transfer metal).

Fig. 3 shows clearly that increasing J brings the DFT+ $U+J$ results into closer agreement with the results of sDFT+ U ($J = 0$) calculations, indicating that in transition metal perovskites the main physical content of the spin-dependent density functionals is an effective

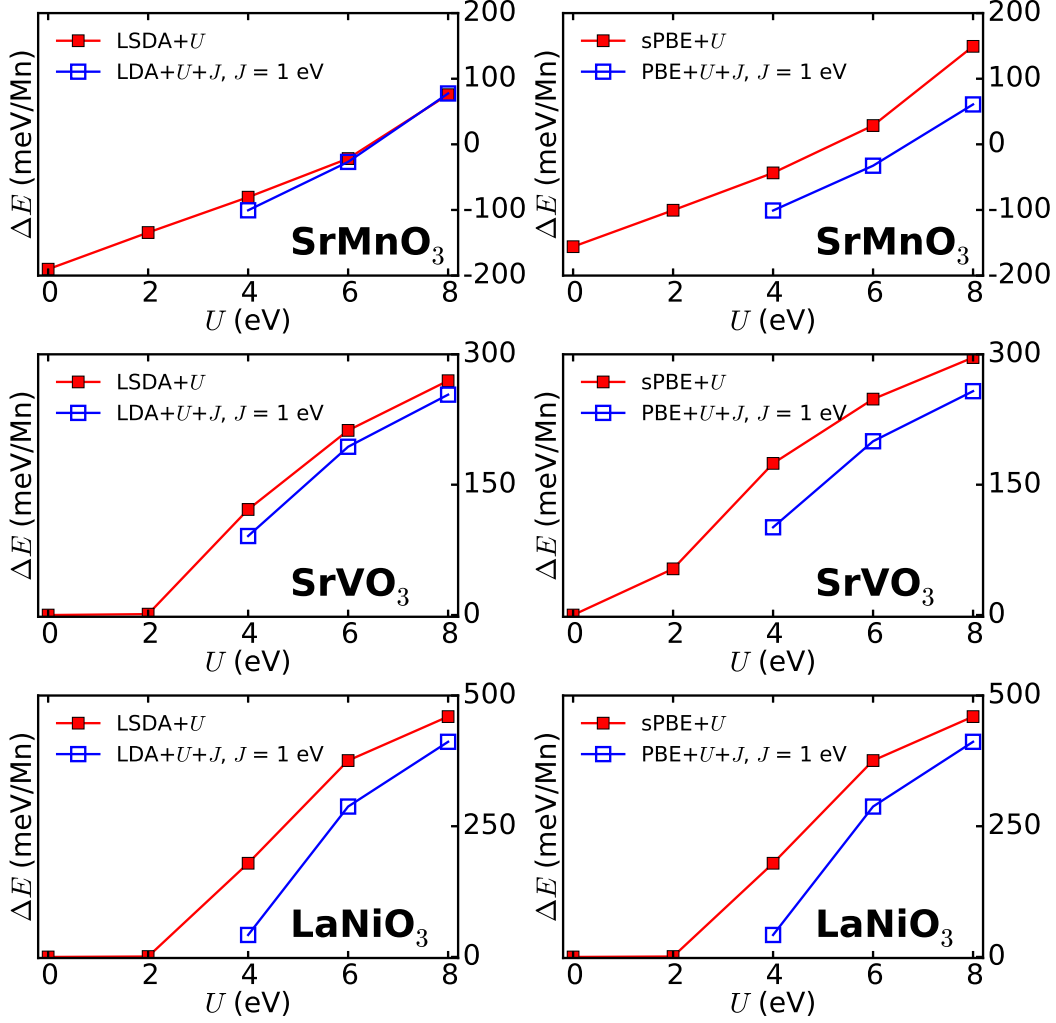


FIG. 3: Comparison of antiferromagnetic-ferromagnetic ground state energy differences obtained using sDFT+ U (closed symbols, red on-line) and DFT+ $U+J$ with $J = 1$ eV (open symbols, blue on-line) for materials indicated. Left panels: LSDA+ U and LDA+ $U+J$ (with $J = 1$ eV). Right panels: sPBE+ U and PBE+ $U+J$ (with $J = 1$ eV).

“ J ” acting on the transition metal d -levels. We may define the size of the effective “ J ” of the sDFT functionals as the J that needs to be added to make the DFT+ $U + J$ results coincide with the sDFT+ U ($J = 0$) results. The effective J is $\gtrsim 1$ eV and is seen to depend on materials and functionals, being larger for sPBE than for sDFT and larger for LaNiO₃ than for SrMnO₃.

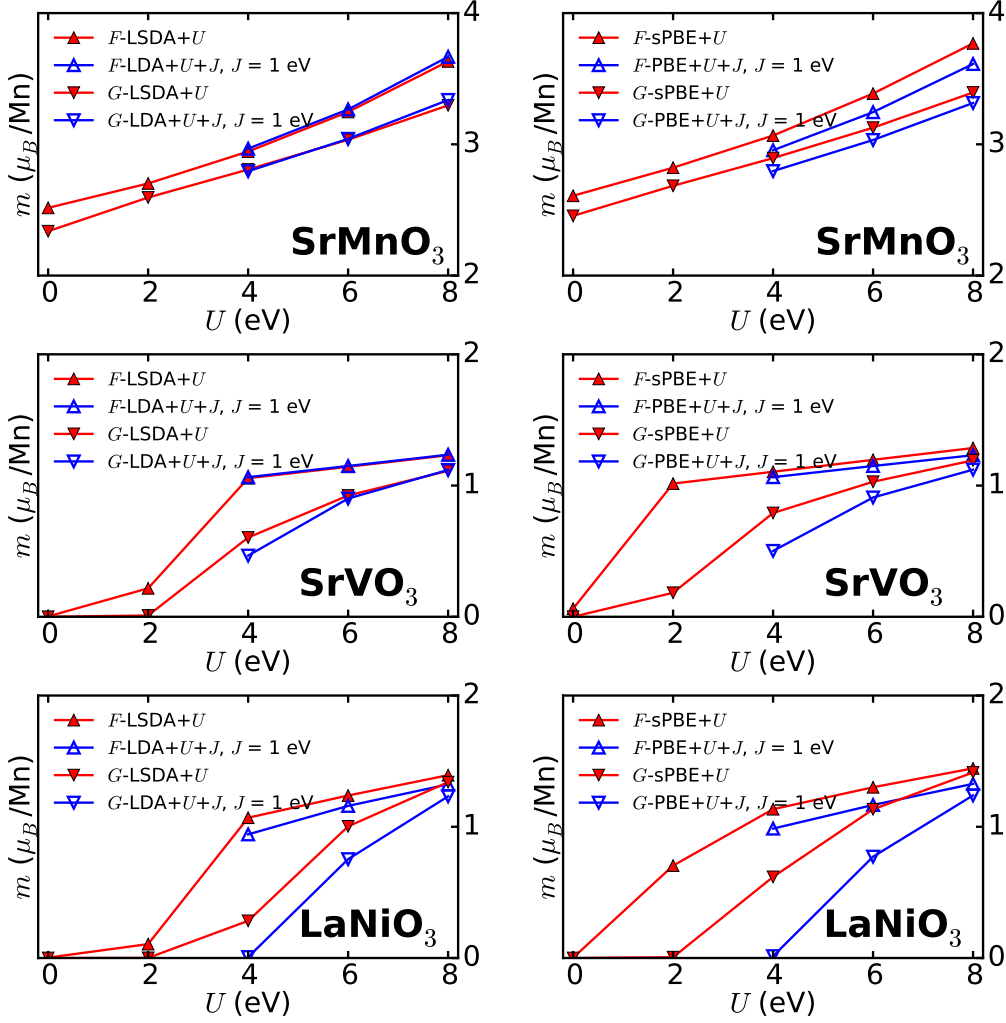


FIG. 4: Comparison of magnetic moments obtained using sDFT+ U (closed symbols, red on-line) and DFT+ $U+J$ with $J = 1$ eV (open symbols, blue on-line) for materials indicated. Left panels: LSDA+ U and LDA+ $U+J$ (with $J = 1$ eV). Right panels: sPBE+ U and PBE+ $U+J$ (with $J = 1$ eV). The upper triangles are for ferromagnetism. The down triangles are for G -type antiferromagnetism.

Fig. 4 shows the magnetic moments of different transition metal oxides, calculated as in Fig. 3 and presented using the same conventions. Consistent with Fig. 3, a J equal to or slightly larger than 1 eV must be added in the spin-independent DFT+ $U+J$ calculations to reproduce the magnetic moments calculated from the sDFT+ U ($J = 0$) method.

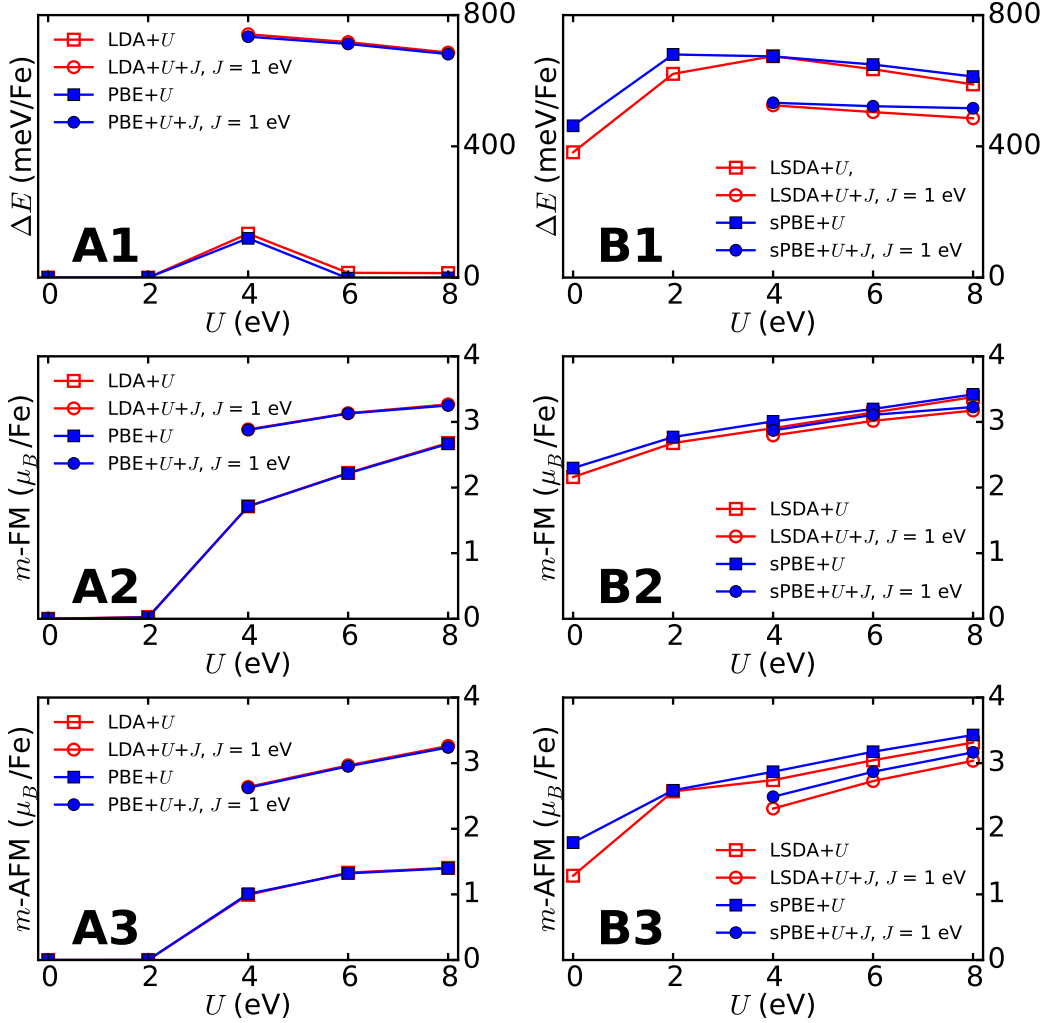


FIG. 5: Comparison of predictions from LDA+ U + J /PBE+ U + J (panels **A**) and LSDA+ U + J /sPBE+ U + J (panels **B**) methods for ground state properties of body-centered Fe. Row 1: energy difference $\Delta E = E(G) - E(F)$ between ferromagnetic (F) and G -type antiferromagnetic (G) ordering. Row 2: magnetic moment per Mn of ferromagnetic state. Row 3: magnetic moment per Mn of G -type antiferromagnetic state.

We next consider Fe, which we study as a representative elemental transition metal. We investigate the extent to which the previous results we obtain from perovskite oxides may apply to transition metals. Fig. 5, which uses the same convention as Fig. 2, presents the antiferromagnetic-ferromagnetic energy difference as well as the local moments in fermag-

netic and antiferromagnetic states for body-centered Fe. Experimentally, the body-centered iron is ferromagnetic with a magnetic moment of $2.2 \mu_B/\text{Fe}$ [39]. The left panels of Fig. 5 show that a Hubbard U less than 4 eV in the DFT+ U + J method does not produce a magnetic ground state for iron, which is inconsistent with experiment. As $U \geq 4$ eV, a magnetic ground state is produced with a sizable magnetic moment on Fe ($> 2\mu_B/\text{Fe}$). As $J = 0$, the ferromagnetic and antiferromagnetic states are almost degenerate for a wide range of Hubbard U . As J is increased from $J = 0$, the ferromagnetic state becomes substantially favored in energy. Similar results were also found for SrMnO_3 and other perovskite oxides. The right panels of Fig. 5 show (also as found in perovskite oxides) that LSDA/sPBE alone ($U = J = 0$) suffices to split the spin and yield a sizable magnetic moment ($\sim 2.2 \mu_B/\text{Fe}$ for ferromagnetism and $\sim 1.5 \mu_B/\text{Fe}$ for antiferromagnetism), which agrees well with the experiment [39]. Increasing U impairs the agreement and increasing J in sDFT+ U + J destabilizes ferromagnetism.

IV. DENSITY OF STATES

In this section, we study the density of states (DOS) obtained using different exchange correlation functionals at $U = 0$ and 6 eV and Hund's coupling $J = 0$ and 1 eV. For ease of interpretation, we present results obtained in the ferromagnetic state. It is useful to analyze the results in terms of the standard phenomenological Slater-Kanamori interaction, which for simplicity we discuss for the simple case of a half-filled fully spin-polarized orbitally symmetric t_{2g} shell treated in the Hartree-Fock (" $+U+J$ ") approximation (this is a simple model for cubic SrMnO_3). In this case the spin up/down potential for each t_{2g} orbital arising from this interaction is:

$$V_\alpha^\uparrow = 2U - 6J \quad (3)$$

$$V_\alpha^\downarrow = 3U - 4J \quad (4)$$

where α labels a t_{2g} orbital (the derivation is in the Appendix). Taking into account the double counting terms, in the DFT+ U + J method, we have:

$$V_\alpha^\uparrow = 2U - 6J - V_{DC} \quad (5)$$

$$V_\alpha^\downarrow = 3U - 4J - V_{DC} \quad (6)$$

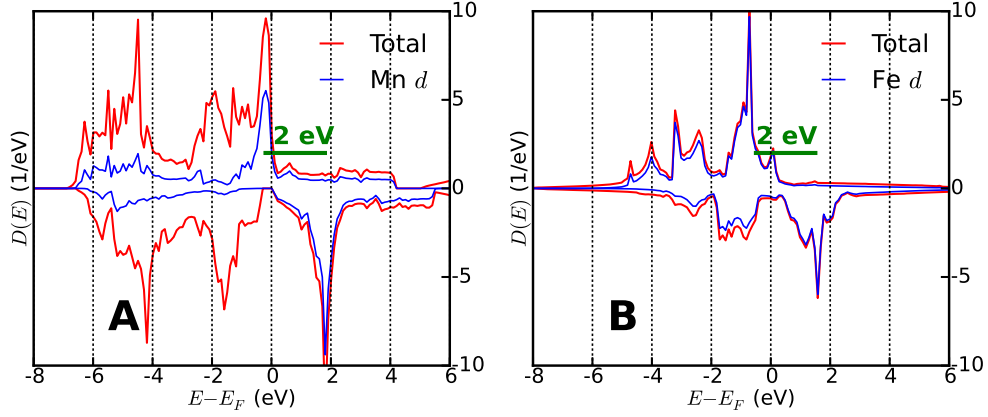


FIG. 6: Density of states of ferromagnetic ordering calculated using the LSDA ($U=J=0$) method. **A)** cubic SrMnO_3 ; **B)** iron. Positive and negative y axis curves show majority and minority density of states, respectively. The horizontal green line and the number provide estimates of the spin splitting.

where the double counting correction V_{DC} is spin-independent. Therefore, in the DFT+ $U+J$ case the energy difference between the spin up and spin down potentials is:

$$|V_{\alpha}^{\uparrow} - V_{\alpha}^{\downarrow}| = U + 2J \quad (7)$$

However, in the sDFT+ $U+J$ method, we have:

$$V_{\alpha}^{\uparrow} = 2U - 6J - V_{DC}^{\uparrow} \quad (8)$$

$$V_{\alpha}^{\downarrow} = 3U - 4J - V_{DC}^{\downarrow} \quad (9)$$

where the double counting correction V_{DC}^{σ} is spin dependent. Therefore, in the sDFT+ $U+J$ case, using the FLL double counting scheme Eq. (2), the energy difference between the spin up and spin down potentials is:

$$|V_{\alpha}^{\uparrow} - V_{\alpha}^{\downarrow}| = |U + 2J - Jm| = |U - J| \quad (10)$$

where $m = N_d^{\uparrow} - N_d^{\downarrow}$ is the magnetization of the d orbitals and in this simple t_{2g} model $m = 3$. This shows that adding J in sDFT+ $U+J$ *reduces* the spin splitting.

Next we present the DFT-computed densities of states in which we find the peaks that are attributable to the d -levels. The energy differences between the majority and minority spin channels then reflect the values of U and J . Fig. 6 presents the pure LSDA densities

of states for ferromagnetic SrMnO₃ and elemental Fe. We see that both materials exhibit a DOS peak at an energy ~ 2 eV above the Fermi level in the minority spin channel and a d -related peak in the majority spin channel slightly below the Fermi level. In SrMnO₃ the d -states visible at energies ~ -4 to -6 eV arise from admixture with oxygen orbitals. We define the spin splitting as the peak-to-peak energy difference between the majority and minority spin d -contributions to the densities of states and indicate it by the heavy green line. For SrMnO₃ the peak to peak splitting of the d -bands provides an estimate of intrinsic “ $2J$ ”, indicating an effective J of about 1 eV. In Fe the interpretation is complicated by the higher occupancy of the d -band (the calculated N_d of Fe is very close to the nominal occupancy of 6).

Fig. 7 presents the density of states for ferromagnetic SrMnO₃ calculated using different exchange correlation functionals. The majority spin density of states has a significant peak between -2 and 0 eV, but this peak has only modest d content. It arises from oxygen p states, with modest p - d hybridization. The main portion of the occupied majority spin d -states occurs much further below the Fermi level, at an energy of -5 to -6 eV with the precise energy depending on the exchange correlation functional. In mathematical terms the double counting correction shifts the mean energy of the d -states down to this low energy (a level repulsion due to hybridization with the oxygen p states also plays a role).

The spin splitting is defined as in the previous case and is again shown as a horizontal bar (green on-line) in Fig. 7. Comparison of Fig. 7**A1** (LDA+ U) and **A2** (LDA+ U + J) shows that adding a J to LDA+ U calculations increases the spin splitting by 2.5 eV, slightly larger than $2J$. The difference arises from a small occupancy of e_g states.

Comparison of Fig. 7**A1** (LDA+ U) and **A2** (LDA+ U + J) to **B1** (LSDA+ U) reveals that even with no added J , the LSDA+ U method produces a larger spin splitting than the LDA+ U + J method with $J = 1$ eV: in other words, the spin dependence of the exchange correlation functional corresponds to an effective $J \gtrsim 1$ eV on the transition metal d orbitals. This is consistent with the estimate of intrinsic “ J ” from pure LSDA spectrum (Fig. 6).

Inspection of Fig. 7**B2** (LSDA+ U + J) reveals that adding a J to the LSDA+ U *reduces* the spin splitting, in contrast to the effect of adding a J to the LDA+ U calculation. This is consistent with the analysis of our simple t_{2g} model. We believe this counterintuitive J dependence in sDFT+ U + J method is a general feature, as was previously noted in the study of a spin-crossover molecule [18]. The underlying origin is that the spin dependence of the

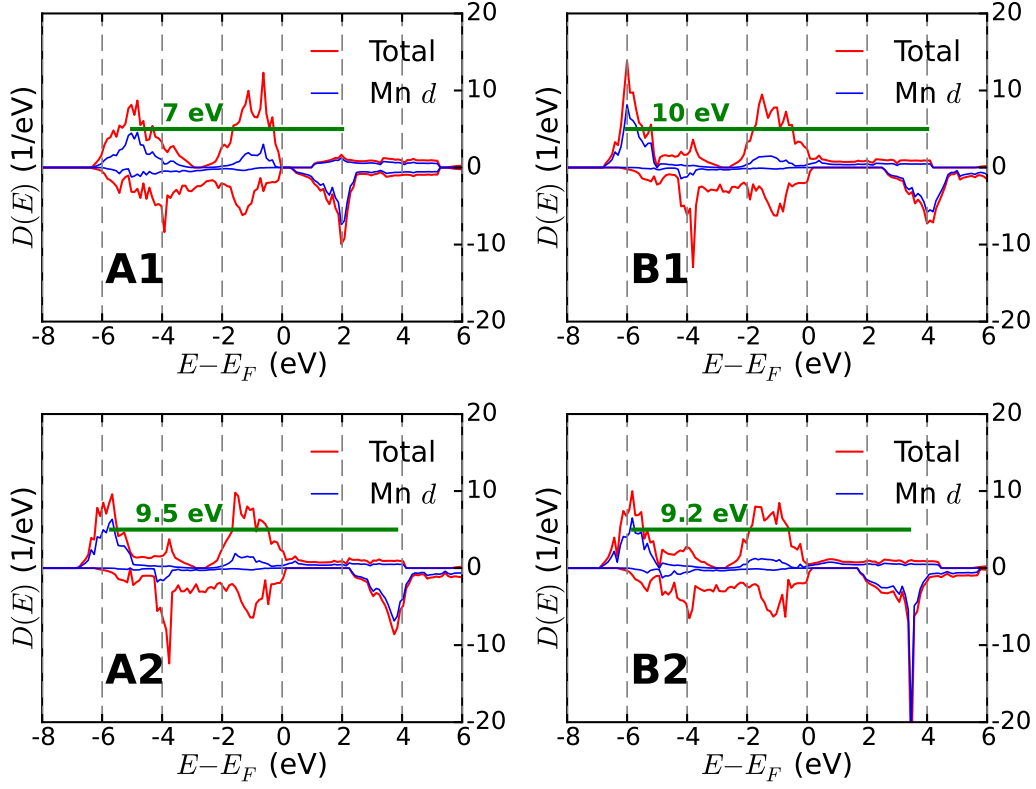


FIG. 7: Total density of states (heavy line, red on-line) and Mn d -projected (light line, blue on-line) of cubic SrMnO₃ in the ferromagnetic state. Positive and negative y axis curves show the majority and minority densities of states, respectively. **A1)** LDA+ U ; **A2)** LDA+ U + J ; **B1)** LSDA+ U ; **B2)** LSDA+ U + J ; $U = 6$ eV and $J = 1$ eV. Horizontal green lines and numbers provide estimates of spin splitting obtained from peak-to-peak separation of majority and minority spin d -density of states peaks.

double counting correction overcompensates for the Hartree shift produced by the J , which is consistent with the trend that increasing J in sDFT+ U + J *destabilizes* ferromagnetism.

Fig. 8 presents the density of states of body-centered Fe. Qualitatively, the variation of spin-splittings predicted by different exchange correlation functionals (LDA+ U \rightarrow LDA+ U + J \rightarrow LSDA+ U \rightarrow LSDA+ U + J) is very similar to that found for cubic ferromagnetic SrMnO₃.

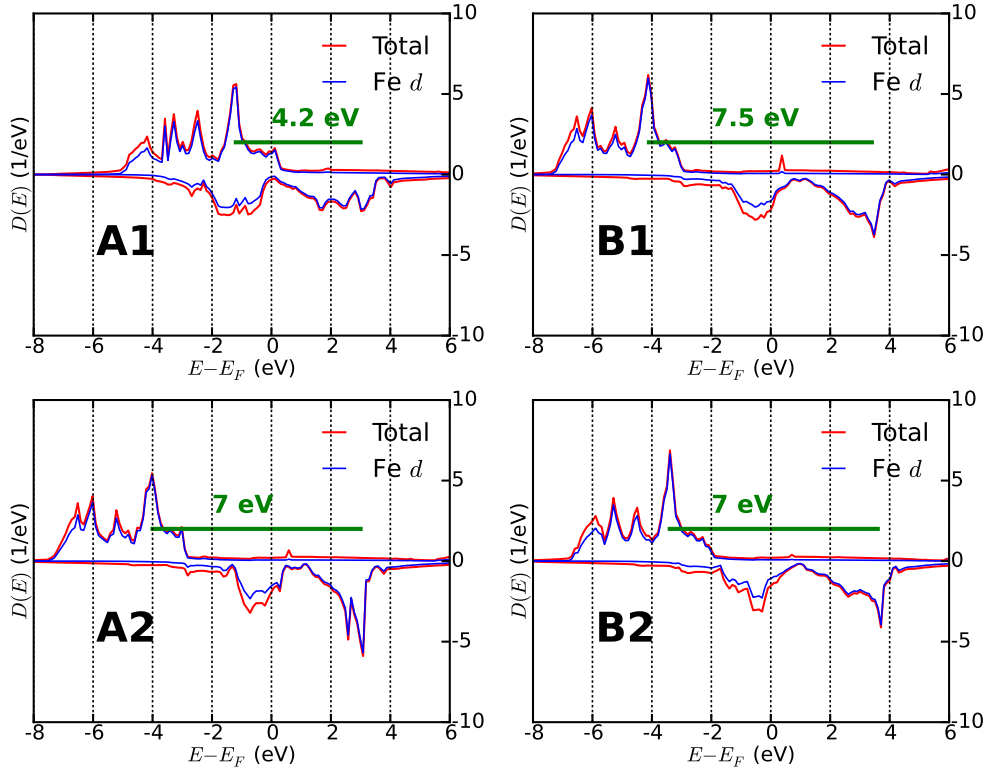


FIG. 8: Density of states of body-centered iron with ferromagnetic ordering, calculated using different exchange correlation functional approximations: **A1**) LDA+ U ; **A2**) LDA+ U + J ; **B1**) LSDA+ U ; **B2**) LSDA+ U + J ; $U = 6$ eV and $J = 1$ eV. Horizontal green lines and numbers provide estimates of spin splitting.

V. CONCLUSIONS

In this paper we have studied energetics and local magnetic moments of representative transition metal oxides (antiferromagnetic Mott insulator SrMnO_3 , moderately correlated metal SrVO_3 and negative charge transfer insulator LaNiO_3) and an elemental transition metal (Fe) to gain further insight into the physics of spin-dependent density functional theories and their “+ U ” and “+ J ” extensions previously noted in Ref. [17]. In these materials, the only states with significant spin polarization are the transition metal d -states and important aspects of the physics are controlled by an exchange splitting of spin configurations of these states. For a transition metal ion in free space, the exchange splitting is convention-

ally described by a Hund’s coupling parameter J and we interpret the exchange splitting found in our calculations as an effective J_{eff} , which may have contributions from the spin dependence of the density functional and from an explicitly added interaction term.

The results are similar for all materials studied. The spin-dependent density functionals are found to encode an exchange splitting in the spin configurations of transition metal d -orbitals, which is larger in the spin-dependent PBE functional (sPBE) than that in the local spin density functional (LSDA) but in both cases is at least 2 eV. Comparison to results of the “ $+U$ ” “ $+J$ ” methods suggests that the J_{eff} corresponding to the spin-dependent density functional is about 1 eV. This value is larger than the range of 0.6-1 eV which is generally accepted as a reasonable estimation for transition metals and their oxides, suggesting that the present implementations of the spin-polarized DFT methods may overestimate the effects of spin polarization in transition metal- d orbitals.

We also found that including an explicit Hund’s coupling J to the spin dependent DFT functional (sDFT+ $U+J$) reduces the calculated exchange splitting below its $J = 0$ value, whereas adding a J to the charge-density-only DFT functional (DFT+ $U+J$) increases the splitting as expected. This counterintuitive J dependence in sDFT+ $U+J$ method arises from the spin-dependence of the double counting correction. The effect was previously noted in the study of LaNiO_3 [17] and was carefully documented in the study of a spin crossover molecule [18]. Our results provide further support for the previous conclusions [17, 18] that while spin-dependent density functionals provide successful descriptions of many materials, caution is needed in their applications to transition metals and their oxides. In particular, for these compounds it is advantageous to base beyond density functional analyses such as the $+U+J$ and +DMFT on spin-independent density functionals (LDA or the PBE-parametrized GGA functional), because the physical meaning of U and J in the parametrization is more clear and the value of J implicit in present implementations of the spin-dependent exchange correlation functionals is likely to be too large.

Appendix A: Derivation of Eqs. (3, 4)

In this section, we derive Eqs. (3, 4). The Hamiltonian of a rotationally invariant Slater-Kanamori (SK) interaction is:

$$\hat{H}_{\text{SK}} = \sum_{\alpha} U \hat{n}_{\alpha\uparrow} \hat{n}_{\alpha\downarrow} + \frac{1}{2} \sum_{\alpha \neq \beta} (U - 2J) \hat{n}_{\alpha\uparrow} \hat{n}_{\beta\downarrow} + \frac{1}{2} \sum_{\alpha \neq \beta, \sigma} (U - 3J) \hat{n}_{\alpha\sigma} \hat{n}_{\beta\sigma} \quad (\text{A1})$$

where α labels a d orbital and σ labels a spin. On the mean-field level, we simply approximate the operator $\hat{n}_{\alpha\sigma}$ as an occupancy $n_{\alpha\sigma}$ and then obtain an energy functional:

$$E = \sum_{\alpha} U n_{\alpha\uparrow} n_{\alpha\downarrow} + \frac{1}{2} \sum_{\alpha \neq \beta} (U - 2J) n_{\alpha\uparrow} n_{\beta\downarrow} + \frac{1}{2} \sum_{\alpha \neq \beta, \sigma} (U - 3J) n_{\alpha\sigma} n_{\beta\sigma} \quad (\text{A2})$$

The potential associated with a given orbital α and a given spin σ is $V_{\alpha}^{\sigma} = \frac{\partial E}{\partial n_{\alpha\sigma}}$. Therefore we have:

$$V_{\alpha}^{\uparrow} = \frac{\partial E}{\partial n_{\alpha\uparrow}} = U n_{\alpha\downarrow} + \sum_{\beta \neq \alpha} (U - 2J) n_{\beta\downarrow} + \sum_{\beta \neq \alpha} (U - 3J) n_{\beta\uparrow} \quad (\text{A3})$$

$$V_{\alpha}^{\downarrow} = \frac{\partial E}{\partial n_{\alpha\downarrow}} = U n_{\alpha\uparrow} + \sum_{\beta \neq \alpha} (U - 2J) n_{\beta\uparrow} + \sum_{\beta \neq \alpha} (U - 3J) n_{\beta\downarrow} \quad (\text{A4})$$

For the simple model of a half-filled fully spin-polarized orbitally symmetric t_{2g} shell, we have three orbitals: $\alpha = d_{xy}, d_{xz}, d_{yz}$ and the occupancy is: $n_{\alpha\uparrow} = 1, n_{\alpha\downarrow} = 0$ for each orbital α . Therefore we have:

$$V_{\alpha}^{\uparrow} = 0 + 0 + 2(U - 3J) = 2U - 6J \quad (\text{A5})$$

$$V_{\alpha}^{\downarrow} = U + 0 + 2(U - 2J) = 3U - 4J \quad (\text{A6})$$

which are Eqs. (3, 4).

Acknowledgments

A. J. Millis is supported by National Science Foundation under grant No. DMR-1308236. H. Chen is supported by National Science Foundation under Grant No. DMR-1120296. A. J. Millis thanks the College de France for hospitality and a stimulating intellectual environment while this paper was being prepared. We thank C. Marianetti, A. Georges, S. Biermann and especially, K. Burke for helpful comments.

[1] R. O. Jones and O. Gunnarsson, Rev. Mod. Phys. **61**, 689 (1989).

- [2] P. Hohenberg and W. Kohn, Phys. Rev. **136**, B864 (1964).
- [3] W. Kohn and L. J. Sham, Phys. Rev. **140**, A1133 (1965).
- [4] U. Vonbarth and L. Hedin, Journal Of Physics Part C Solid State Physics **5**, 1629 (1972).
- [5] S. K. Ma and B. Brueckner, Physical Review **165**, 18 (1968).
- [6] R. Rajagopal and J. Callaway, Phys. Rev. B **7**, 1912 (1973).
- [7] O. Gunnarsson and B. I. Lundqvist, Phys. Rev. B **13**, 4274 (1976).
- [8] M. Rasolt, Phys. Rev. B **16**, 3234 (1977).
- [9] M. Rasolt and H. L. Davis, Physics Letters A **86**, 45 (1981).
- [10] M. Imada, A. Fujimori, and Y. Tokura, Rev. Mod. Phys. **70**, 1039 (1998).
- [11] V. I. Anisimov, J. Zaanen, and O. K. Andersen, Phys. Rev. B **44**, 943 (1991).
- [12] A. I. Liechtenstein, V. I. Anisimov, and J. Zaanen, Phys. Rev. B **52**, R5467 (1995).
- [13] A. Georges, Lectures on the Physics of Highly Correlated Electron Systems VIII: Eighth Training Course in the Physics of Correlated Electron Systems and High-Tc Superconductors **715**, 3 (2004).
- [14] G. Kotliar, S. Y. Savrasov, K. Haule, et al., Rev. Mod. Phys. **78**, 865 (2006).
- [15] K. Held, I. A. Nekrasov, G. Keller, V. Eyert, N. Bluemer, A. K. McMahan, R. T. Scalettar, T. Pruschke, V. I. Anisimov, and D. Vollhardt, Phys. Status Solidi **243**, 2599 (2006).
- [16] H. Park, A. J. Millis, and C. A. Marianetti, Phys. Rev. B **89**, 245133 (2014).
- [17] H. Park, A. J. Millis, and C. A. Marianetti, Phys. Rev. B **92**, 035146 (2015).
- [18] J. Chen, A. J. Millis, and C. A. Marianetti, Phys. Rev. B **91**, 241111 (2015).
- [19] J. H. Lee and K. M. Rabe, Phys. Rev. Lett. **104**, 207204 (2010).
- [20] J. M. Rondinelli, A. S. Eidelson, and N. A. Spaldin, Phys. Rev. B **79**, 205119 (2009).
- [21] K. Haule, Phys. Rev. Lett. **115**, 196403 (2015).
- [22] M. T. Czyżyk and G. A. Sawatzky, Phys. Rev. B **49**, 14211 (1994).
- [23] M. Karolak, G. Ulm, T. Wehling, V. Mazurenko, A. Poteryaev, and A. Lichtenstein, Journal of Electron Spectroscopy and Related Phenomena **181**, 11 (2010).
- [24] J. P. Perdew, K. Burke, and M. Ernzerhof, Phys. Rev. Lett. **77**, 3865 (1996).
- [25] R. Søndena, S. Stølen, P. Ravindran, and T. Grande, Phys. Rev. B **75**, 214307 (2007).
- [26] T. Maekawa, K. Kurosaki, and Y. S., J. Alloys Compd. **426**, 46 (2006).
- [27] K.-S. Hwang and B.-H. Kim, Journal of the Korean Physical Society **34**, 51 (1999).
- [28] W. P. Davey, Phys. Rev. **25**, 753 (1925).

- [29] M. C. Payne, M. P. Teter, D. C. Allan, T. A. Arias, and J. D. Joannopoulos, *Rev. Mod. Phys.* **64**, 1045 (1992).
- [30] G. Kresse and J. Furthmüller, *Phys. Rev. B* **54**, 11169 (1996).
- [31] P. E. Blöchl, *Phys. Rev. B* **50**, 17953 (1994).
- [32] G. Kresse and D. Joubert, *Phys. Rev. B* **59**, 1758 (1999).
- [33] T. Takeda and S. Ohara, *J. Phys. Soc. Jpn* **37**, 275 (1974).
- [34] W. Luo, A. Franceschetti, M. Varela, J. Tao, S. J. Pennycook, and S. T. Pantelides, *Phys. Rev. Lett.* **99**, 036402 (2007).
- [35] J. D. Burton and E. Y. Tsymbal, *Phys. Rev. B* **80**, 174406 (2009).
- [36] H. Chen and S. Ismail-Beigi, *Phys. Rev. B* **86**, 024433 (2012).
- [37] H. Chen, Q. Qiao, M. S. J. Marshall, A. B. Georgescu, A. Gulec, P. J. Phillips, R. F. Klie, F. J. Walker, C. H. Ahn, and S. Ismail-Beigi, *Nano Letters* **14**, 4965 (2014).
- [38] L. Vaugier, H. Jiang, and S. Biermann, *Phys. Rev. B* **86**, 165105 (2012).
- [39] T. Crangle and G. C. Hallam, *Proceedings of the Royal Socieity of London. Series A, Mathematical and Physical Sciences* **272**, 119 (1963).